



# Effect of solution chemistry and aggregation on adsorption of perfluorooctanesulphonate (PFOS) to nano-sized alumina<sup>★</sup>

Jun-Meng Jian<sup>a</sup>, Chi Zhang<sup>b</sup>, Fen Wang<sup>a</sup>, Xingwen Lu<sup>c</sup>, Fei Wang<sup>a,\*</sup>, Eddy Y. Zeng<sup>a</sup>

<sup>a</sup> Guangdong Key Laboratory of Environmental Pollution and Health, School of Environment, Jinan University, Guangzhou 510632, China

<sup>b</sup> Department of Geology, The University of Kansas, 304 Lindley Hall, 1475 Jayhawk Blvd., Lawrence, KS 66045-7575, USA

<sup>c</sup> School of Environmental Science and Engineering, Guangdong University of Technology, Guangzhou, 510006, China

## ARTICLE INFO

### Article history:

Received 2 February 2019

Received in revised form

15 April 2019

Accepted 6 May 2019

Available online 8 May 2019

### Keywords:

PFOS

Adsorption

Nanomaterial

Aggregation

Dynamic light scattering

Shape

## ABSTRACT

The interaction of pollutants with nanomaterials has attracted attention due to the extensive application of nanomaterials. In this study, the adsorption behavior of PFOS on nano-alumina with different shapes was investigated. First, the adsorption isotherms and kinetics of PFOS on alumina nanoparticles (NPs) and nanowires (NWs) were measured to calculate thermodynamic parameters. The effects of solution chemistry (e.g., pH, ionic strength, and the presence of humic acid) on adsorption were further studied. The different aggregation behavior of alumina NPs and NWs were the critical factor for PFOS adsorption, as demonstrated through dynamic light scattering (DLS) experiments. This study is the first to investigate the aggregation effects on PFOS adsorption on nanomaterials and the results should be useful in identifying the important roles of shape and aggregation of nanomaterials on the fate of organic pollutants in the environment.

© 2019 Elsevier Ltd. All rights reserved.

## 1. Introduction

Perfluorooctanesulphonate (PFOS) is a persistent and bio-accumulative organic pollutant commonly found in the environment and in biota, and was added as a Persistent Organic Pollutant in Annex B of the Stockholm Convention in 2009 (Paul et al., 2009). The properties of PFOS include high chemical and thermal stability, low surface free energy and surface activity (Hekster et al., 2003; Lehmler, 2005; Schultz et al., 2003). It has been impregnated in carpets, furniture, paper and textiles, as well as in fire-fighting materials. Over 122,500 tons of perfluorooctylsulfonate fluoride (POSF, a major precursor of PFOS) were produced globally between 1972 and 2002 (Paul et al., 2009). PFOS can also be produced from the degradation of their precursors. Direct emissions from POSF-containing products have released 450–2700 tons of PFOS into the aquatic environment (Paul et al., 2009).

Sorption, reverse osmosis and nanofiltration are currently accepted methods for the removal of PFOS from water. Sorption of PFOS to various materials, especially granular activated carbon, has been reported to be more economical than other removal

techniques such as reverse osmosis and some forms of advanced oxidation (Deng et al., 2015). For example, Valeria et al. (2008) reported that sorption to activated carbon could consistently remove 90% of PFOS in aqueous solution. However, the search for sorbents with high selectivity and lower cost for removal of PFOS is ongoing.

It is reported that PFOS may interact with nanomaterials in the environment, which could affect its fate and distribution (Kwadijk et al., 2013). Nanomaterials have been applied well beyond the laboratory into the commercial marketplace, and have been increasingly applied in industrial processes due to their unique electronic, optical, thermal and photoactive properties (Aitken et al., 2006; Baur and Silverman, 2007; Colvin, 2003; Liu, 2006). Inevitably, nanomaterials are released to the environment. It is necessary to elucidate their interactions with environmental pollutants to predict their dispersion, transport, aggregation, and deposition in aquatic environments. Among all common nanomaterials, alumina is one of the top ten engineered nanoparticles in terms of production (Piccinno et al., 2012). Because of their widespread use in a variety of areas, alumina nanomaterials are commonly detected in aquatic environments (Keller et al., 2013). Their presence in the aquatic environment may affect the fate and transport of sorbed pollutants (Petersen et al., 2011). Although numerous studies have investigated adsorption of pollutants on alumina nanomaterials (Franco et al., 2014; Nadafi et al., 2014; Onnby et al., 2014; Qian et al., 2014, 2015; Srivastava et al., 2011;

<sup>★</sup> This paper has been recommended for acceptance by Baoshan Xing.

\* Corresponding author.

E-mail address: [wf1984@jnu.edu.cn](mailto:wf1984@jnu.edu.cn) (F. Wang).

Tabesh et al., 2018; Yang et al., 2010), most have only examined the adsorption efficiency (Franco et al., 2014; Onnby et al., 2014; Tabesh et al., 2018). The mechanisms of pollutant adsorption on NPs remain poorly defined. So far, only one study investigated the adsorption mechanism of PFOS on different nano-sized inorganic oxides (Lu et al. (2016b)).

Besides solution chemistry, the behavior of nanomaterials in water is largely dependent on colloidal properties such as particle size and surface charge of nanomaterials (Lowry et al., 2012; Petosa et al., 2010). Compared to larger alumina particles, nano-sized alumina has a greater tendency to aggregate in aqueous solution (Safonov et al., 2010; Witharana et al., 2012). Aggregation kinetics has been considered an influential factor in the mobility and environmental fate of various nanomaterial systems (Baalousha, 2017; Batley et al., 2013; Raza et al., 2016). Aggregation can lead to an increase in the effective hydrodynamic diameter of nanoparticles in water, a key property affecting the adsorption of pollutants. In addition, the surface charge of suspended nanoparticles in water affects aggregation ability.

To fill the above-mentioned knowledge gap, the present study used alumina NPs and NWs as representative nanomaterials to explore the adsorption behavior of PFOS on nanomaterials of different shapes. The adsorption kinetics and isotherms were examined experimentally and theoretically. The aggregation behavior of NPs and NWs under different pH values, ionic strengths and HA concentrations were analyzed with dynamic light scattering to quantify aggregation behavior. The present study was the first to investigate the aggregation effects on PFOS adsorption on nanomaterials, and the results are useful for identifying the role of shape and aggregation of nanomaterials in the fate of organic pollutants in the environment.

## 2. Materials and methods

### 2.1. Materials and material characterization

Humic acid, ammonium acetate for high pressure liquid chromatography–tandem mass spectrometry (HPLC/MS/MS) analysis and PFOS were purchased from Sigma-Aldrich. Sodium perfluoro- $^{13}\text{C}_8$ -octanesulfonate (M8PFOS) was purchased from Wellington Laboratories (Guelph, Canada). Sodium chloride was purchased from Xilong Chemical (Guangdong, China). Premium pure methanol was purchased from Fisher Scientific (Geel, Belgium).

Alumina NPs and NWs were purchased from Sigma-Aldrich. X-ray diffraction (XRD) using an X-ray Powder Diffractometer (D8 Advance, Bruker) revealed that the alumina NPs and NWs were dominated by  $\theta$ -alumina and  $\delta$ -alumina phases, respectively (Fig. S1). The surface areas of alumina NPs and NWs were  $83.0\text{ m}^2\text{ g}^{-1}$  and  $124.9\text{ m}^2\text{ g}^{-1}$  as determined by a Brunauer-Emmett-Teller ( $\text{N}_2$  adsorption) surface area analyzer (Coulter SA 3100, Beckman Coulter). The particle size of alumina NPs was 13 nm, while the diameter and length of alumina NWs were 2–6 and 13 nm, respectively. The zeta-potentials of alumina NPs and NWs at selected pH values were analyzed with a zeta-potential analyzer (Coulter Delsa 440SX, Beckman Coulter). The point of zero charge ( $\text{pH}_{\text{pzc}}$ ) was 9.8 and 10.5 for alumina NPs and NWs, respectively. Surface morphology was elucidated with a Hitachi S-4800 scanning electron microscope (SEM) equipped with a secondary electron detector (Fig. S2).

### 2.2. Aggregation experiments

Dynamic light scattering (DLS) was used to study the aggregation behavior of alumina NP and NW. A Nano ZS 90 (Malvern

Instruments) was used to investigate particle size distributions in solutions with different pH values, ionic strength and humic acid concentrations. The experimental conditions in DLS tests were kept consistent with adsorption experiment before the DLS analysis. Each sample (with different solution chemistry) was measured in triplicate.

### 2.3. Sorption experiments

Based on preliminary testing with different amounts of sorbents and sorbate, 6 mg NPs and 40 mg NWs were used in the adsorption experiments. The alumina NP or NW solutions were then mixed with 40 ml PFOS solution at an initial concentration of  $50\text{ }\mu\text{g/L}$  in 50 ml polypropylene copolymer (PPCO) Nalgene centrifuge tubes. Each tube was placed on a shaker at 200 rpm at  $25\text{ }^\circ\text{C}$  for 4 h. In the kinetic sorption experiment, tubes were shaken from 5 to 480 min (5, 10, 20, 30, 60, 120, 240, and 480 min, respectively). In the equilibrium isotherm experiment, the initial PFOS concentration was 10–1000  $\mu\text{g/L}$  (10, 20, 30, 50, 100, 200, 300, 500, and 1000  $\mu\text{g/L}$ ), at 30, 40 and  $50\text{ }^\circ\text{C}$ . The effect of solution pH on PFOS adsorption was conducted at pH values from 4 to 10, using 0.1 M HCl and 0.1 M NaOH to adjust pH. To evaluate the effect of ionic strength, different concentrations of 0.001–0.1 M  $\text{NaCl}_{(\text{aq})}$  (0.001, 0.005, 0.01, 0.05, and 0.1 M) were introduced. Similarly, different amounts of humic acid ranging from 0 to 50 mg/L were used. All experiments were run in three duplicates.

### 2.4. Determination of PFOS and HA

After the adsorption experiments, the solution mixture was centrifuged at 9000 rpm for 20 min. Then 2.5 ml of supernatant was collected and diluted with 2.5 ml methanol. The diluted mixture was filtered through a  $0.2\text{ }\mu\text{m}$  Whatman inorganic membrane filter (Maidstone, UK) to remove particulate and colloidal material prior to PFOS analysis. The initial 3 ml of filtered mixture was discarded to avoid the potential effect of membrane adsorption.

Chromatography was done using an Eclipse Plus C18 column (2.1 i.d.  $\times$  100 mm long,  $1.8\text{ }\mu\text{m}$ , Agilent). Milli-Q water ( $18\text{ M}\Omega\text{-cm}$ ) containing 0.1% formic acid (v/v) and methanol were used as mobile phases A and B at a flow rate of 0.2 ml/min. The injection volume was 5  $\mu\text{l}$ . The gradient started with 75% A and 25% B, was linearly ramped to 25% A and 75% B over 3 min, then ramped to 0% A and 100% B over 1 min and held for 2 min, then ramped to 75% A and 25% B. The column was allowed to equilibrate for 0.1 min, and the total running time was 7.1 min. The amount of PFOS were determined by an ultra-performance liquid chromatography (Nexera X2, Shimadzu) equipped with a tandem mass spectrometer (Triple Quad<sup>TM</sup> 5500 System, AB SCIEX) operating in electrospray negative ionization mode. The tandem MS analysis was conducted using multiple reaction monitoring (MRM) mode, and the cone voltage and collision energy were  $-60\text{ V}$  and  $-90\text{ V}$ , respectively. In addition, 10 ml supernatant was transferred from the adsorption tube to a glass bottle for total organic carbon (TOC) analysis. The concentration of HA in the post-adsorption solution was analyzed by a TOC analyzer (Vario TOC, Elementar).

### 2.5. Quality assurance and quality control

Sodium perfluoro-1- $^{13}\text{C}_8$ -octanesulfonate (M8PFOS) was used to test the recovery rate of the entire sorption procedure. The recoveries of the internal standards of M8PFOS were  $88 \pm 7\%$ . To reduce the potential loss of PFOS during the sorption process, two blank samples were set with three sorption samples at the same sorption conditions (e.g. temperature and solution chemistry). The adsorbed amount of PFOS on alumina nanomaterials was

determined by subtracting the average concentration in sorption samples from the average blank sample concentration.

### 3. Results and discussion

#### 3.1. Adsorption kinetic and isotherm

The adsorption kinetics of PFOS on alumina NP and NW at pH 6.0 are shown in Fig. 1, and indicates that adsorption was fast and that equilibrium was reached within 30 min. It is also suggested that there was no intra-particle diffusion occurred during the adsorption process due to the small size of alumina nanomaterials (Nassar, 2010). Nassar (2010) showed that the adsorption of asphaltenes onto alumina nanoparticles needed 2 h to reach equilibrium. Besides the possible adsorption behavior difference between PFOS and asphaltenes, this longer adsorption equilibrium time might be attributed to the much higher initial concentration of asphaltenes used in the study of Nassar (2010) which is almost 2000 times higher than our study. We applied two commonly used kinetic models, pseudo first-order (Eq. (1)) and pseudo second-order (Eq. (2)), to evaluate the adsorption kinetic data:

$$\ln(q_e - q_t) = \ln q_e - k_1 t \tag{1}$$

$$\frac{t}{q_t} = \frac{1}{k_2 q_e^2} + \frac{1}{q_e} \tag{2}$$

where  $q_e$  (mg/g) and  $q_t$  (mg/g) are the amounts of PFOS adsorbed per unit mass of the adsorbent at equilibrium and at time ( $t$ ), respectively; and  $k_1$  and  $k_2$  are the rate constants of the pseudo first and second-order models, respectively (Table 1). The results showed that the adsorption of PFOS on NP and NW are fitted slightly better with the second pseudo-order model. It is clear that PFOS adsorption on NP is greater than that on NW, which indicates that the shape of nanomaterials may be important for pollutant adsorption.

Temperature is an important environmental factor for stability, aggregation state, and adsorption efficiency of nanomaterials (Baalousha, 2017; Pacek et al., 2007; Zhang et al., 2012). The adsorption isotherms of PFOS on NPs and NWs at 30 °C, 40 °C and 50 °C are shown in Fig. 2. The data was also fitted using two isotherm models, the Langmuir and Freundlich equations (Haring,

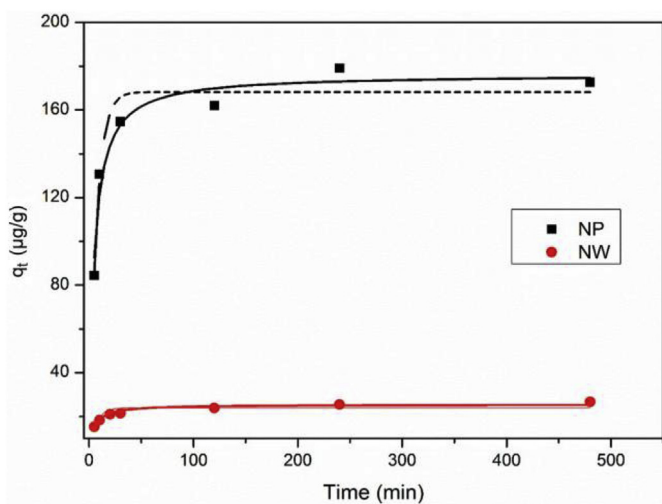


Fig. 1. The adsorption kinetics of PFOS on alumina NP and NW at pH 6.0 ± 0.2 (the solid line is the fit of the pseudo first-order model and the dashed line is the fit of the pseudo second-order kinetic model).

Table 1  
Constants of the pseudo first-order and pseudo second-order kinetic models fitting for the adsorption of PFOS on alumina NPs and NWs.

alumina nanomaterial		NP	NW
Pseudo first-order	$k_1$ (min <sup>-1</sup> )	0.142	0.165
	$q_e$ (g/g)	168	24.0
	$R^2$	0.937	0.905
Pseudo second-order	$k_2$ (g/g•min)	0.00125	0.0103
	$q_e$ (g/g)	176	25.5
	$R^2$	0.948	0.939

1926; Langmuir, 1918), and the fitting parameters are shown in Table 2:

Langmuir model:

$$q_e = \frac{K_L q_m C_e}{1 + K_L C_e} \tag{3}$$

Freundlich model:

$$q_e = K_F C_e^{\frac{1}{n}} \tag{4}$$

where  $q_e$  is the amount of the adsorbate on the surface of the adsorbent at equilibrium (mg/g),  $C_e$  is the equilibrium

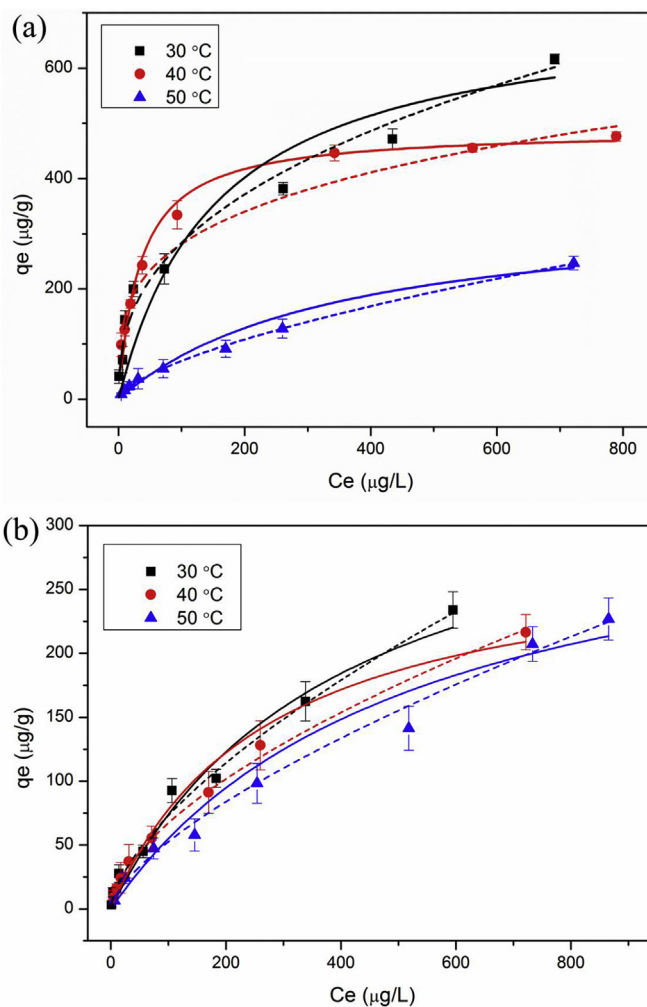


Fig. 2. The adsorption isotherms of PFOS on NP and NW at pH 6.0 ± 0.2 (the solid line is the fit of the Langmuir model and the dash line is the fit of the Freundlich model).

**Table 2**  
 Constants of the Langmuir and Freundlich equations fitting for the adsorption of PFOS on alumina NPs and NWs, and the calculated thermodynamic data.

alumina nanomaterial		NP			NW		
T(°C)		30	40	50	30	40	50
Langmuir constants							
	$K_L$ (L/g)	0.013	0.030	0.0017	0.0025	0.0037	0.0019
	$q_m$ (mg/g)	589	485	447	368	288	343
	$R^2$	0.890	0.981	0.983	0.961	0.969	0.971
Freundlich constants							
	$K_F$ [(mg/g)(g/L) <sup>-n</sup> ]	47.8	85.3	3.57	3.71	4.29	2.37
	$n$	2.60	3.73	1.56	1.56	1.68	1.49
	$R^2$	0.980	0.949	0.998	0.985	0.998	0.992
	$\Delta G^0$ (kJ/mol)	-23.9	-26.8	-19.9	-19.7	-21.4	-20.3
	$\Delta H^0$ (kJ/mol)		-84.6			-11.4	
	$\Delta S^0$ (kJ/mol•K)		-0.190			0.029	

concentration of the adsorbate in solution (mg/L),  $q_m$  is the maximum adsorption capacity (mg/g),  $K_L$  is the Langmuir adsorption constant (L/mg),  $K_F$  is the Freundlich adsorption constant [(mg/g)(mg/L)<sup>-n</sup>], and  $n$  represents the heterogeneity factor.

For the adsorption of PFOS on both alumina NP and NW, the data are fitted well with both the Langmuir and Freundlich equations (Table 2). With regards to the derived constants of the Freundlich model, the values of  $n$  (1.49–3.73) at all three temperatures (30, 40, and 50 °C) were all greater than 1, suggesting surface adsorption of PFOS on alumina NP and NW. Meanwhile, the  $q_m$  values of PFOS adsorption on alumina NPs and NWs were from 288 to 589 mg/g, which are much higher than those on macro-sized alumina (Wang and Shih, 2011; Wang et al., 2012). In addition, the results showed that the  $q_m$  of PFOS adsorption on NP (589, 485, and 447 mg/g) were all higher than those on NW (368, 288, and 343 mg/g) (Table 2), which should be attributed to the different shape of NP and NW. The mechanisms will be analyzed in the following sections with more evidences. Temperature affected the aggregation by affecting the random Brownian motion of particles and the collision frequency (Zhang et al., 2012).

The following equations (Eq. (5) and Eq. (6)) were used to evaluate the thermodynamic parameters of adsorption ( $\Delta G^0$ ,  $\Delta H^0$ , and  $\Delta S^0$ ), which are summarized in Table 2:

$$\Delta G^0 = -RT \ln(K_d) \quad (5)$$

$$\Delta G^0 = \Delta H^0 - T\Delta S^0 \quad (6)$$

where  $R$  is the gas constant,  $T$  is the absolute temperature, and  $K_d$  is the adsorption equilibrium constant ( $K_L$  in the Langmuir equation).  $\Delta G^0$ ,  $\Delta H^0$ , and  $\Delta S^0$  are the changes in Gibbs free energy, enthalpy, and entropy of adsorption, respectively.

Usually,  $\Delta G$  is used to represent physical (-20 to 0 kJ/mol) and chemical (-400 to -80 kJ/mol) sorption (Vimonses et al., 2009). In this study, all the  $\Delta G$  values were negative and around -20 kJ/mol (Table 2), indicating that the sorption of PFOS on alumina NP and NW is favorable, exothermic, and is predominately through physical sorption. It might be due to the presence of spontaneity and absence of energy barrier during the adsorption of PFOS. The negative entropy ( $\Delta S^0$ ) indicates that the adsorption of PFOS on alumina NP was constant without further modification of structures at the solid-liquid interface. The negative entropy also indicated that the reorientation or restructuring of water around the solute or surface was favorable (Chang et al., 2009). The positive value of  $\Delta S^0$  implied the increase of randomness at the solid/solution interface during PFOS sorption. The increase in the randomness may be associated with the fact that the adsorbed water molecules was replaced by PFOS. Such a process would gain

more translational entropy for the displaced water molecules, which allows the prevalence of randomness in the system.

### 3.2. Effect of solution chemistry

Solution chemistry can be critical for the adsorption of pollutants on nanomaterials (Engel and Chefetz, 2016; Gora and Andrews, 2017; Lu et al., 2016a; Mwaanga et al., 2014; Zhu et al., 2014) and usually plays an important role on the aggregation behavior of nanomaterials, which will affect adsorption on their surfaces (Chen et al., 2008; Cho et al., 2011; Ma and Uddin, 2013; Rosenzweig et al., 2014; Shih and Wang, 2013). The effects of pH, ionic strength, and the presence of humic acid are described below.

#### 3.2.1. Effect of pH

The effects of pH on PFOS adsorption on alumina NP and NW are shown in Fig. 3(a). The adsorption levels of PFOS on alumina NP and NW were both decreased as the pH increases. When the pH increased from 4.0 to 10.0, the adsorbed amount of PFOS on alumina NP decreased moderately from 230 to 100 mg/mg, but dramatically decreased on alumina NW from 25 to 0 mg/mg. The point of zero charge of alumina NP and NW were both around 10.0 (Fig. S4). When the pH increased from 4.0 to 10.0, the surface charge would decrease due to the neutralization of positive charge with OH<sup>-</sup>. When the electrostatic interaction between PFOS particle and alumina nanomaterial played a dominant role in the adsorption process, the adsorption level should decrease to be around 0. Such proposed phenomena was observed for alumina NW, but the adsorption level of PFOS on alumina NP was still around 100 mg/mg at pH 10. It was proposed that the stronger aggregation of alumina NP than NW was the key factor for such observation (Fig. 5). When the pH increased to 10 (around the  $pH_{pzc}$ ), the surface charge of alumina NP was around 0 at pH 10 (Fig. S4), electrostatic interaction can be ignored. The strong PFOS adsorption on alumina NP at pH 10 should be caused by the potential aggregation of NPs, which can trap PFOS molecules in the NP aggregates (Fig. 3). Although alumina NWs can still form big aggregates at pH 10 (Fig. 5(a)), the loose structures may limit the trap of PFOS molecules (Fig. 6). This may be the reason why PFOS adsorption on alumina NW decreased to around 0 when pH increased to 10 (no electrostatic attraction occurred).

#### 3.2.2. Effect of ionic strength

In Fig. 3(b), it is clear that PFOS adsorption on both alumina NP and NW decreased with increasing ionic strength. Adak et al. (2005) proposed that increasing the ionic strength may increase the adsorption of ionic surfactants on alumina, given the potential reduction in the lateral repulsive force between the head groups of two adjacent ionic surfactant molecules. However, much lower

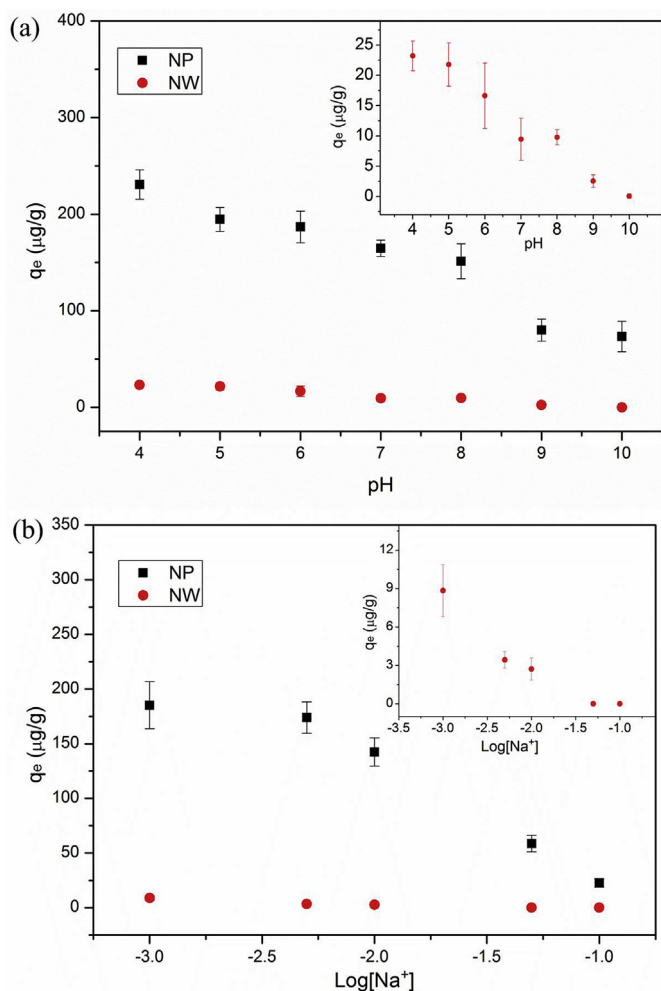


Fig. 3. The effects of pH and ionic strength on PFOS adsorption on NPs and NWs.

concentrations of PFOS were used in this study, and thus the reduction effect of the lateral repulsive force could generally be ignored. It is also possible that the electrostatic attraction between the positively charged alumina surface and the negatively charged PFOS molecules was reduced due to the compression of the electrical double layer and a reduction in zeta-potential (Wang et al., 2012; Wang and Shih, 2011).

The potential effects of ionic strength on the aggregation stage of nanomaterials also need to be specified. In general, ionic strength influences the aggregation as the interaction energy barrier  $E_b$  is dependent on ionic strength. The  $E_b$  must be overcome by random movement of NPs in order to orient collisions effectively for successful aggregation (Chen et al., 2011; Kumar et al., 2012). As the ionic strength increases, the  $E_b$  decreases to lower the inter-particle repulsion to facilitate aggregation. At high ionic strength, the electrical double layer (EDL) could collapse to drive aggregation, therefore the effective surface area of adsorption decreases to result in a lower adsorption.

Fig. 5(c) and (d) shows that the aggregate diameter of both alumina NP and NW increased with the increase of ionic strength. Since alumina NP and NW both have net positive surface charges at the used pH (around 7.0) in ionic effects, electrostatic repulsion between two positively-charged NPs and two positively-charged NWs would be critical to the aggregate behavior. From the perspective of DLVO theory, an increase in ionic strength will compress the electric double layer on the surface of NPs and NWs,

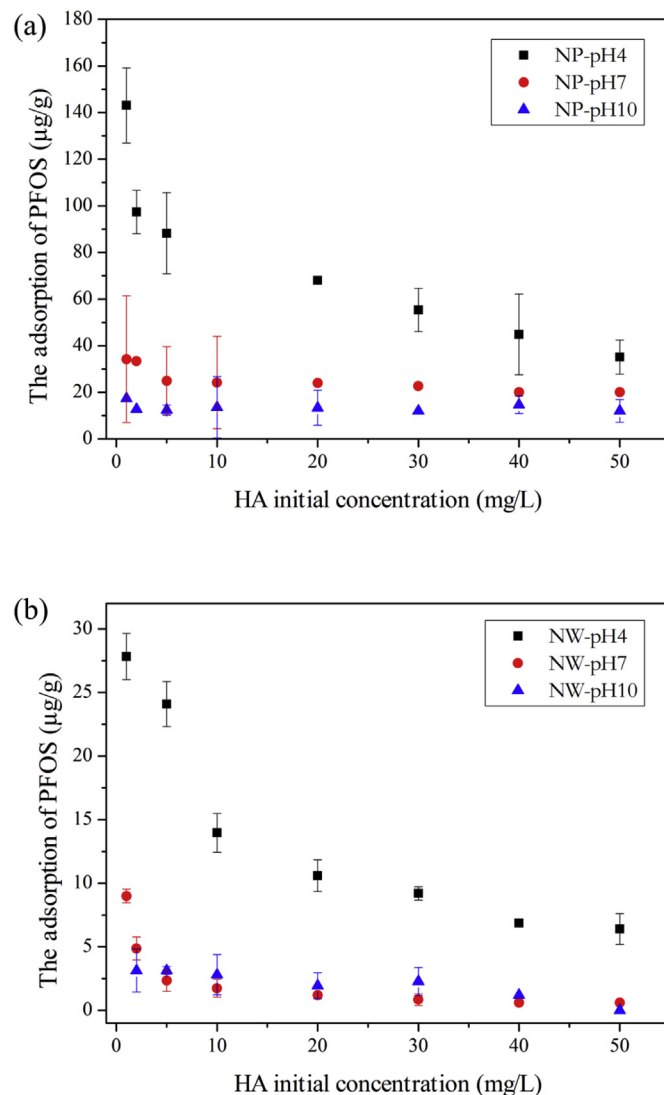


Fig. 4. The effects of HA concentrations on PFOS adsorption on NPs and NWs at different pH (4, 7, and 10).

which would further screen the electrostatic repulsion between them and increase their aggregate diameters. Accordingly, an increase in the aggregate diameter of alumina NPs should increase PFOS adsorption. However, PFOS adsorption also decreased significantly with the increase of ionic strength (Fig. 3(b)). It should be point that alumina NPs with positive charge should be looser than without charge on the surface due to exist of electrostatic repulsion. Therefore, PFOS adsorbed by aggregated alumina NPs at higher ionic strength should be weak. Furthermore, it is well-known that the increase of ionic strength will greatly reduce electrostatic attraction between alumina surface and PFOS molecule. Thus, PFOS adsorption on alumina NPs decreased quickly with the increase of ionic strength.

### 3.2.3. Effect of humic acid

Natural organic matter, including HA, is commonly found in environmental systems such as soils, as well as surface and sub-surface waters. HAs have a great influence on the surface charge of mineral particles. HA has been reported to impact the aggregation of nanoparticles associated with its adsorption onto nanoparticles (Zhu et al., 2014), and the adsorption of HA and its effect on the

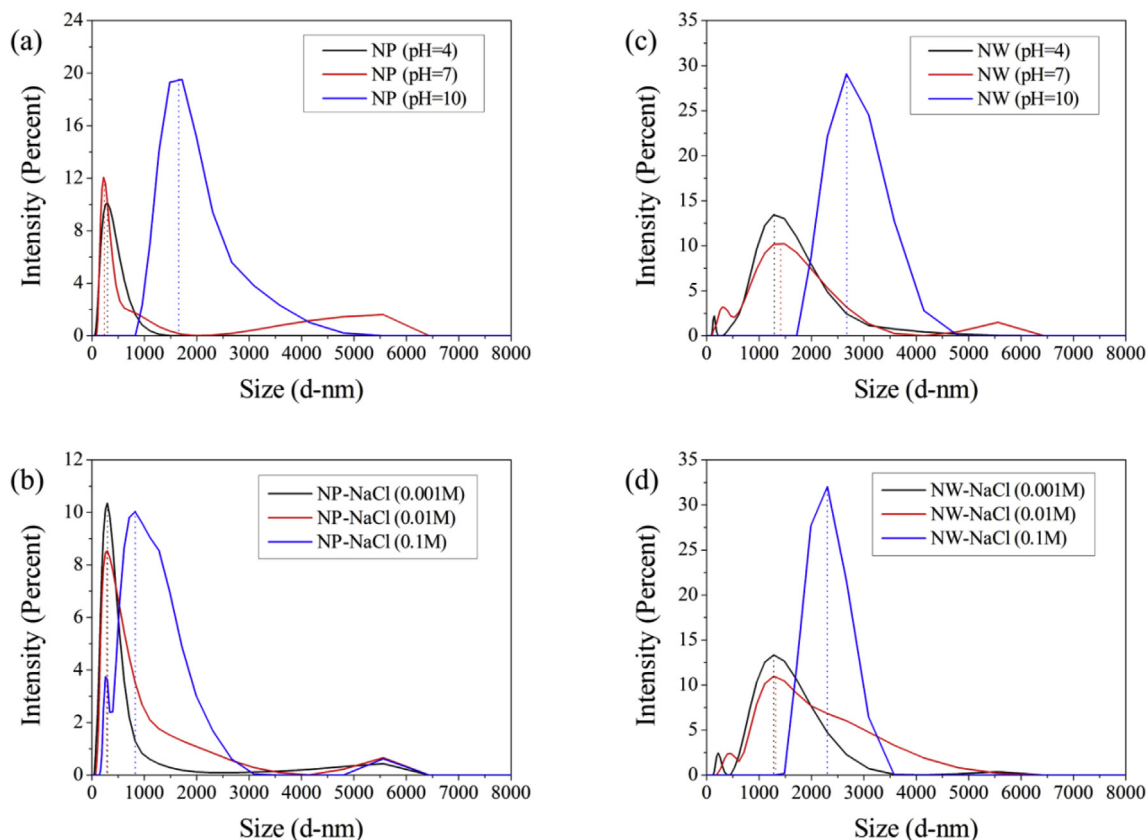


Fig. 5. Intensity-based size distribution of alumina NPs and NWs at different pH (a, c) and ionic strength (b, d) by dynamic light scattering.

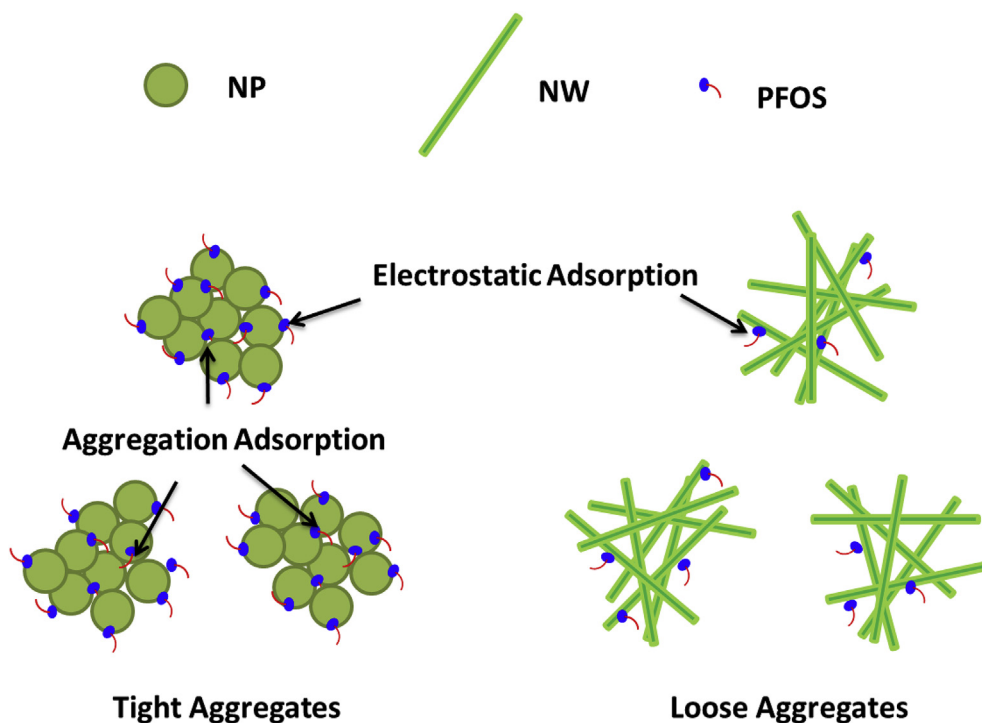


Fig. 6. The conceptual models for the different adsorption mechanism between alumina NP and NW towards PFOS.

surface charge and the colloidal stability of several oxides have been studied (Han et al., 2017; Liu et al., 2018). The pH-dependent effects of humic acid on the adsorption of PFOS on alumina NP and

NW at three different pH values (4.0, 7.0, and 10.0) are shown in Fig. 4. Generally, HA had a negative effect on PFOS adsorption on both alumina NP and NW, with dramatically decreasing PFOS

adsorption with increasing humic acid concentration. We attributed such decreases to the competition of HA and PFOS for the positive charge on the alumina surface. Furthermore, the adsorbed HA on alumina surface may also repel PFOS adsorption due to electrostatic repulsion.

One obvious phenomenon was greater adsorption of PFOS at pH 4 than at pH 7 and 10 at the same HA concentration. A lower pH can greatly increase the positive sites on the alumina surface. Although HA adsorbed more readily to the more abundant positive sites under lower values of pH, the sorption of PFOS on both alumina nanomaterials also increased for the same reason. Furthermore, a lower pH can also protonate the acidic functional groups in HA, thereby facilitating aggregation of HA on the alumina surface (Fig. S5). This neutralization of the negatively-charged HA would reduce the electrostatic repulsion between PFOS and the HA-modified surface of nano-alumina. Hence, PFOS may more readily

sorb to HA aggregates on the surfaces of alumina nanomaterials by partitioning (Wang et al., 2015).

The potential effects of HA on the aggregation of alumina NP and NW would also affect PFOS adsorption on alumina. Fig. 7 illustrates the effect of HA on the aggregate diameter of alumina NP and NW. At pH 4.0, the increase in HA concentration increased the aggregate diameter of alumina NP and NW first, then their aggregate diameters decreased with further increases of HA concentrations. The increase in aggregate diameter should be caused by the neutralization of positive charge on the surfaces of NPs and NWs due to adsorption of HA. The resulting reduction of electrostatic repulsion between the NPs and NWs will greatly increase their aggregation. Furthermore, HA molecules usually carry numerous negative charges, which can act as bridges for NPs and NWs. However, at higher concentrations of HA, the surfaces of NP or NW become negatively charged. Under such conditions, the electrostatic

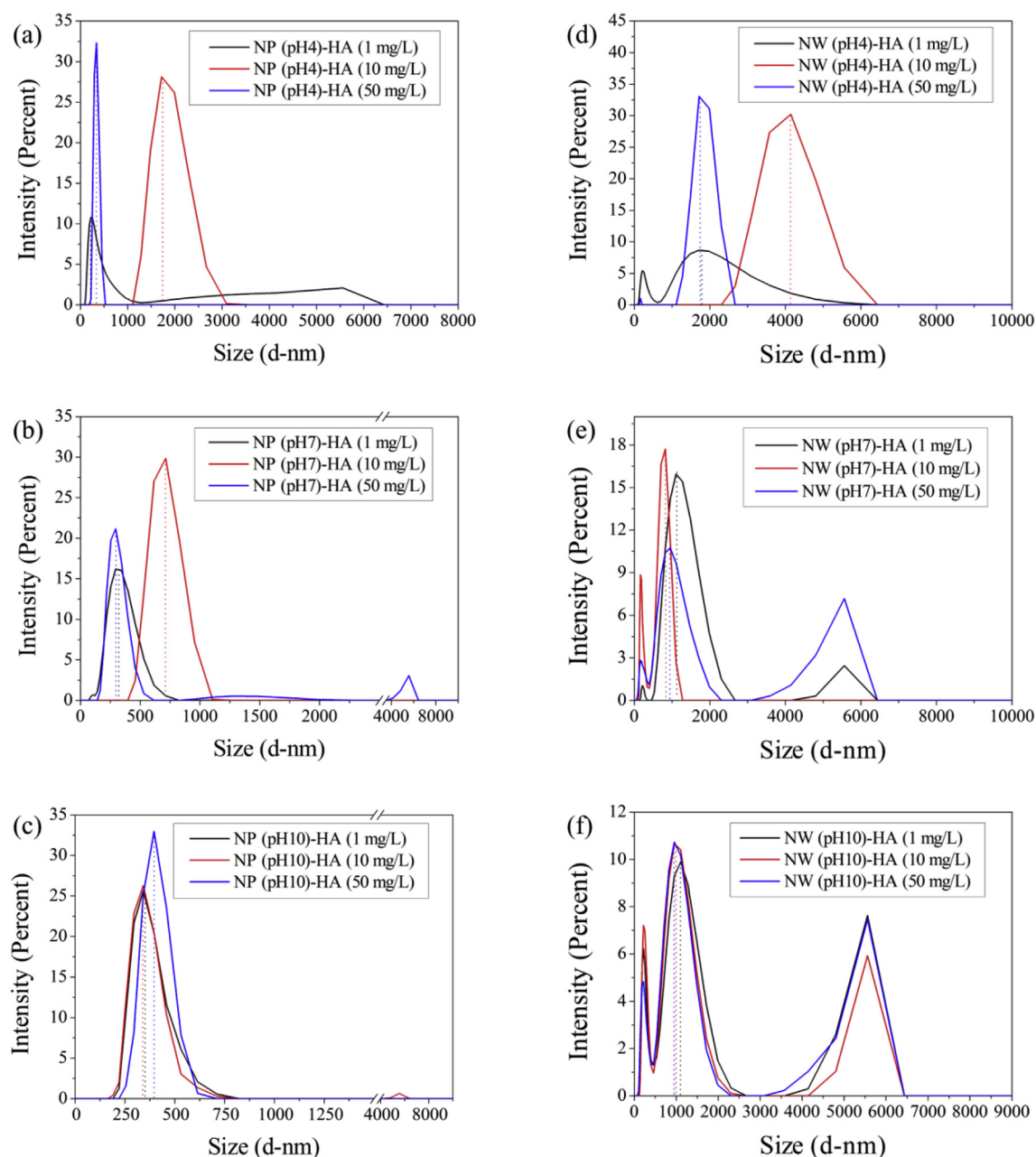


Fig. 7. Intensity-based size distribution of alumina NPs (a, b, c) and NWs (d, e, f) at different pH and HA concentrations by DLS.

repulsion between NPs or NWs may inhibit aggregation, which was observed as smaller particles at the highest HA concentration studied (50 mg/L) (Fig. 7(a) and (b)). Meanwhile, PFOS adsorption decreased continuously with increases in HA concentration from 1.0 to 50.0 mg/L at pH 4.0 regardless of the aggregation diameter of either type of nano-alumina. These findings suggest that the competitive adsorption of HA with PFOS was the dominant mechanism for the decrease in PFOS adsorption on alumina NP and NW at pH 4.0. However, the adsorption of PFOS decreased more slowly, when HA increased from 20.0 to 50.0 mg/L. Previous study (CITE REFS) suggested that some negatively-charged functional groups, such as carboxylates, of HA adsorbed on a mineral surface could be protonated at low pH. This would reduce the electrostatic repulsion between the negatively-charged PFOS molecule and the adsorbed HA on alumina surfaces. PFOS may then partition on the adsorbed HA. At pH 7.0, the effect of HA on the aggregate diameter of alumina NP was similar to that at pH 4.0. However, the effect of HA on the aggregate diameter of alumina NW was not obvious. Similar results were also observed for both NP and NW at pH 10.0. The reason could be the lower adsorption of PFOS at higher pH, which had a more limited effect on the surface charge of alumina nanomaterials. For HA effect on PFOS adsorption on alumina NP and NW, the result showed that PFOS adsorption level on alumina NP and NW all hold without significant changes at pH 7.0 and 10.0. Such observation further indicated that PFOS may partition on the adsorbed HA on alumina NP and NW surfaces.

### 3.3. Analysis of particle properties

Because nanoparticles are so small (less than 100 nm), their interaction with each other can be quite different than that of larger, micrometer-sized particles. These unique nanoscale particle interaction features can greatly affect their adsorption behavior towards PFOS. In our previous studies (Wang et al., 2012; Wang and Shih, 2011), the adsorption of PFOS on normal size of  $\gamma$ -alumina and boehmite were investigated, respectively. Kinetic studies showed that PFOS adsorption on common-sized  $\gamma$ -alumina and boehmite reached equilibrium within 48 h. In contrast, adsorption of PFOS on nano-sized alumina in the current study only needed 30 min to achieve equilibrium. The different kinetic is attributed to higher active sites on the surface of nano-sized than common-sized alumina. The PFOS molecule can be attached on more abundant and higher active sites of nano-sized alumina more readily and quickly. Furthermore, the  $q_m$  of PFOS on common-sized  $\gamma$ -alumina and boehmite were reported to be 0.252 and 0.877 mg/m<sup>2</sup> at 25 °C, respectively. For nano-sized alumina, the maximum adsorption capacity of PFOS on NPs and NWs was calculated to be 7.09 and 2.94 mg/m<sup>2</sup> at 30 °C, which are approximately 28 and 12 times greater than common-sized alumina respectively. Clearly, then, there is a (nano) particle size dependent difference in PFOS sorption behavior to alumina. It is well-known that the surface of nano-material usually has more unsaturated sites, which are active for adsorption. Although  $q_m$  (mg/g) of alumina were normalized with surface area, capacities of nano alumina were still several times of common-sized alumina for each unit area. Changes in particle size or shape (NP vs NW) could potentially explain the possible observed sorption behavior, by exposing different parts of the alumina surface environment or 'reactive' surface area to solution. From the crystal structure perspective,  $\gamma$ -alumina has a more stable crystal structure than boehmite and the two types of nano-alumina studied here (d-alumina NP and q-alumina NW). Boehmite, d-alumina and q-alumina usually contains more defects on the surface. These defects may be easily protonated to be active sites for PFOS adsorption. Both the crystal structure and the nanoparticle size provided important evidence to support the more active sites

on nanomaterials than common-sized materials.

## 4. Conclusions

PFOS can quickly adsorb on the surface of alumina NP and NW, with kinetic data that fit both pseudo first-order and pseudo second-order models. For the adsorption of PFOS on both alumina NP and NW, the data are fitted well with both the Langmuir and Freundlich models. The negative values of  $\Delta G^0$  and  $\Delta H^0$  both showed that the adsorption of PFOS on alumina NP and NW were exothermic. The adsorption levels of PFOS on alumina NP and NW both decreased as the pH and ionic strength increased. The presence of HA showed a strong retardant effect on PFOS adsorption on alumina NP and NW. Based on all the results, the aggregation effect was proposed to be critical for pollutant adsorption on nanomaterials.

## Acknowledgments

This research was supported by Guangdong (China) Innovative and Entrepreneurial Research Team Program (No. 2016ZT06N258), and the National Natural Science Foundation of China (Project No. 21637001 and Project No. 41503087).

## Appendix A. Supplementary data

Supplementary data to this article can be found online at <https://doi.org/10.1016/j.envpol.2019.05.025>.

## References

- Adak, A., Bandyopadhyay, M., Pal, A., 2005. Adsorption of anionic surfactant on alumina and reuse of the surfactant-modified alumina for the removal of crystal violet from aquatic environment. *J. Environ. Sci. Health - Part A Toxic/Hazard. Subst. Environ. Eng.* 40, 167–182.
- Aitken, R.J., Chaudhry, M.Q., Boxall, A.B.A., Hull, M., 2006. Manufacture and use of nanomaterials: current status in the UK and global trends. *Occup. Med.* 56, 300–306.
- Baalousha, M., 2017. Effect of nanomaterial and media physicochemical properties on nanomaterial aggregation kinetics. *Nanoimpact* 6, 55–68.
- Batley, G.E., Kirby, J.K., McLaughlin, M.J., 2013. Fate and risks of nanomaterials in aquatic and terrestrial environments. *Acc. Chem. Res.* 46, 854–862.
- Baur, J., Silverman, E., 2007. Challenges and opportunities in multifunctional nanocomposite structures for aerospace applications. *MRS Bull.* 32, 328–334.
- Chang, Y., Lv, X., Zha, F., Wang, Y., Lei, Z., 2009. Sorption of p-nitrophenol by anion-cation modified polygorskite. *J. Hazard Mater.* 168, 826–831.
- Chen, G., Liu, X., Su, C., 2011. Transport and retention of TiO<sub>2</sub> rutile nanoparticles in saturated porous media under low-ionic-strength conditions: measurements and mechanisms. *Langmuir* 27, 5393–5402.
- Chen, J., Chen, W., Zhu, D., 2008. Adsorption of nonionic aromatic compounds to single-walled carbon nanotubes: effects of aqueous solution chemistry. *Environ. Sci. Technol.* 42, 7225–7230.
- Cho, H.H., Huang, H., Schwab, K., 2011. Effects of solution chemistry on the adsorption of ibuprofen and triclosan onto carbon nanotubes. *Langmuir* 27, 12960–12967.
- Colvin, V.L., 2003. The potential environmental impact of engineered nanomaterials. *Nat. Biotechnol.* 21, 1166–1170.
- Deng, S., Yao, N., Du, Z., Qian, H., Meng, P., Wang, B., Huang, J., Gang, Y., 2015. Enhanced adsorption of perfluorooctane sulfonate and perfluorooctanoate by bamboo-derived granular activated carbon. *J. Hazard Mater.* 282, 150–157.
- Engel, M., Chefetz, B., 2016. Adsorption and desorption of dissolved organic matter by carbon nanotubes: effects of solution chemistry. *Environ. Pollut.* 213, 90–98.
- Franco, C.A., Nassar, N.N., Cortes, F.B., 2014. Removal of oil from oil-in-saltwater emulsions by adsorption onto nano-alumina functionalized with petroleum vacuum residue. *J. Colloid Interface Sci.* 433, 58–67.
- Gora, S.L., Andrews, S.A., 2017. Adsorption of natural organic matter and disinfection byproduct precursors from surface water onto TiO<sub>2</sub> nanoparticles: pH effects, isotherm modelling and implications for using TiO<sub>2</sub> for drinking water treatment. *Chemosphere* 174, 363–370.
- Han, Y., Hwang, G., Park, S., Gomez-Flores, A., Jo, E., Eom, I.-C., Tong, M., Kim, H.-J., Kim, H., 2017. Stability of carboxyl-functionalized carbon black nanoparticles: the role of solution chemistry and humic acid. *Environ. Sci. Nano* 4, 800–810.
- Haring, M.M., 1926. Colloid and capillary chemistry (Freundlich, Herbert). *J. Chem. Educ.* 3.
- Hekster, F.M., Laane, R., de Voogt, P., 2003. Environmental and toxicity effects of

- perfluoroalkylated substances. *Rev. Environ. Sci. Technol.* 179, 99–121.
- Keller, A.A., McFerran, S., Lazareva, A., Suh, S., 2013. Global life cycle releases of engineered nanomaterials. *J. Nano Res.* 15, 1692.
- Kumar, P., Kumar, A., Lead, J.R., 2012. Nanoparticles in the Indian environment: known, unknowns and awareness. *Environ. Sci. Technol.* 46, 7071.
- Kwadijk, C.J.A.F., Velzeboer, I., Koelmans, A.A., 2013. Sorption of perfluorooctane sulfonate to carbon nanotubes in aquatic sediments. *Chemosphere* 90, 1631–1636.
- Langmuir, I., 1918. The adsorption of gases on plane surfaces of glass, mica and platinum. *J. Chem. Phys.* 40, 1361–1403.
- Lehmler, H.J., 2005. Synthesis of environmentally relevant fluorinated surfactants - a review. *Chemosphere* 58, 1471–1496.
- Liu, J., Dai, C., Hu, Y., 2018. Aqueous aggregation behavior of citric acid coated magnetite nanoparticles: effects of pH, cations, anions, and humic acid. *Environ. Res.* 161, 49–60.
- Liu, W.-T., 2006. Nanoparticles and their biological and environmental applications. *J. Biosci. Bioeng.* 102, 1–7.
- Lowry, G.V., Gregory, K.B., Apte, S.C., Lead, J.R., 2012. Transformations of nanomaterials in the environment. *Environ. Sci. Technol.* 46, 6893–6899.
- Lu, J., Liu, D., Yang, X., Liu, H., Liu, S., Tang, H., Zhao, Y., Cui, F., 2016a. Sedimentation of TiO<sub>2</sub> nanoparticles in aqueous solutions: influence of pH, ionic strength, and adsorption of humic acid. *Desalin. Water. Treat.* 57, 18817–18824.
- Lu, X., Deng, S., Wang, B., Huang, J., Wang, Y., Yu, G., 2016b. Adsorption behavior and mechanism of perfluorooctane sulfonate on nanosized inorganic oxides. *J. Colloid Interface Sci.* 474, 199–205.
- Ma, X., Uddin, S., 2013. Desorption of 1,3,5-trichlorobenzene from multi-walled carbon nanotubes: impact of solution chemistry and surface chemistry. *Nanomaterials* 3, 289–302.
- Mwaanga, P., Carraway, E.R., Schlautman, M.A., 2014. Preferential sorption of some natural organic matter fractions to titanium dioxide nanoparticles: influence of pH and ionic strength. *Environ. Monit. Assess.* 186, 8833–8844.
- Nadafi, K., Vosoughi, M., Asadi, A., Borna, M.O., Shirmardi, M., 2014. Reactive red 120 dye removal from aqueous solution by adsorption on nano-alumina. *J. Water Chem. Technol.* 36, 125–133.
- Nassar, N.N., 2010. Asphaltene adsorption onto alumina nanoparticles: kinetics and thermodynamic studies. *Energy Fuels* 24, 4116–4122.
- Onbny, L., Kumar, P.S., Sigfridsson, K.G.V., Wendt, O.Y., Carlson, S., Kirsebom, H., 2014. Improved arsenic(III) adsorption by Al<sub>2</sub>O<sub>3</sub> nanoparticles and H<sub>2</sub>O<sub>2</sub>: evidence of oxidation to arsenic(V) from X-ray absorption spectroscopy. *Chemosphere* 113, 151–157.
- Pacek, A.W., Ding, P., Utomo, A.T., 2007. Effect of energy density, pH and temperature on de-aggregation in nano-particles/water suspensions in high shear mixer. *Powder Technol.* 173, 203–210.
- Paul, A.G., Jones, K.C., Sweetman, A.J., 2009. A first global production, emission, and environmental inventory for perfluorooctane sulfonate. *Environ. Sci. Technol.* 43, 386–392.
- Petersen, E.J., Zhang, L., Mattison, N.T., O'Carroll, D.M., Whelton, A.J., Uddin, N., Tinh, N., Huang, Q., Henry, T.B., Holbrook, R.D., Chen, K.L., 2011. Potential release pathways, environmental fate, and ecological risks of carbon nanotubes. *Environ. Sci. Technol.* 45, 9837–9856.
- Petosa, A.R., Jaisi, D.P., Quevedo, I.R., Elimelech, M., Tufenkji, N., 2010. Aggregation and deposition of engineered nanomaterials in aquatic environments: role of physicochemical interactions. *Environ. Sci. Technol.* 44, 6532–6549.
- Piccinno, F., Gottschalk, F., Seeger, S., Nowack, B., 2012. Industrial production quantities and uses of ten engineered nanomaterials in Europe and the world. *J. Nano Res.* 14, 1109.
- Qian, L., Ma, M., Cheng, D., 2014. The effect of water chemistry on adsorption and desorption of U(VI) on nano-alumina. *J. Mol. Liq.* 197, 295–300.
- Qian, L., Ma, M., Cheng, D., 2015. Adsorption and desorption of uranium on nano goethite and nano alumina. *J. Radioanal. Nucl. Chem.* 303, 161–170.
- Raza, G., Amjad, M., Kaur, I., Wen, D., 2016. Stability and aggregation kinetics of titania nanomaterials under environmentally realistic conditions. *Environ. Sci. Technol.* 50, 8462–8472.
- Rosenzweig, S., Sorial, G.A., Sahle-Demessie, E., Mcavoy, D.C., Hassan, A.A., 2014. Effect of chloride ions and water chemistry on copper(II) adsorption on functionalized and pristine carbon nanotubes compared to activated carbon F-400. *Water Air Soil Pollut.* 225, 1913.
- Safronov, A.P., Leiman, D.V., Blagodetev, D.N., Kotov, Y.A., Bagazeev, A.V., Murzakaev, A.M., 2010. Aggregation of air-dry alumina powder nanoparticles redispersed in an aqueous medium. *Nanotechnol. Russ* 5, 777–785.
- Schultz, M.M., Barofsky, D.F., Field, J.A., 2003. Fluorinated alkyl surfactants. *Environ. Eng. Sci.* 20, 487–501.
- Shih, K., Wang, F., 2013. Adsorption behavior of perfluorochemicals (PFCs) on boehmite: influence of solution chemistry. *Procedia Environ. Sci.* 18, 106–113.
- Srivastava, V., Weng, C.H., Singh, V.K., Sharma, Y.C., 2011. Adsorption of nickel ions from aqueous solutions by nano alumina: kinetic, mass transfer, and equilibrium studies. *J. Chem. Eng. Data* 56, 1414–1422.
- Tabesh, S., Davar, F., Loghman-Estarki, M.R., 2018. Preparation of gamma-Al<sub>2</sub>O<sub>3</sub> nanoparticles using modified sol-gel method and its use for the adsorption of lead and cadmium ions. *J. Alloy. Comp.* 730, 441–449.
- Valeria, O.H., Reyes, S.A., Arpad, S., Jacobsen, N.E., Wysocki, V.H., Field, J.A., 2008. Reductive defluorination of perfluorooctane sulfonate. *Environ. Sci. Technol.* 42, 3260–3264.
- Vimonses, V., Lei, S., Jin, B., Chowd, C.W.K., Saint, C., 2009. Kinetic study and equilibrium isotherm analysis of Congo Red adsorption by clay materials. *Chem. Eng. J.* 148, 354–364.
- Wang, F., Liu, C., Shih, K., 2012. Adsorption behavior of perfluorooctane sulfonate (PFOS) and perfluorooctanoate (PFOA) on boehmite. *Chemosphere* 89, 1009–1014.
- Wang, F., Shih, K., 2011. Adsorption of perfluorooctane sulfonate (PFOS) and perfluorooctanoate (PFOA) on alumina: influence of solution pH and cations. *Water Res.* 45, 2925–2930.
- Wang, F., Shih, K., Leckie, J.O., 2015. Effect of humic acid on the sorption of perfluorooctane sulfonate (PFOS) and perfluorobutane sulfonate (PFBS) on boehmite. *Chemosphere* 118, 213–218.
- Witharana, S., Hodges, C., Xu, D., Lai, X., Ding, Y., 2012. Aggregation and settling in aqueous polydisperse alumina nanoparticle suspensions. *J. Nano Res.* 14, 1–11.
- Yang, K., Zhu, L., Xing, B., 2010. Sorption of phenanthrene by nanosized alumina coated with sequentially extracted humic acids. *Environ. Sci. Pollut. Res.* 17, 410–419.
- Zhang, W., Crittenden, J., Li, K., Chen, Y., 2012. Attachment efficiency of nanoparticle aggregation in aqueous dispersions: modeling and experimental validation. *Environ. Sci. Technol.* 46, 7054–7062.
- Zhu, M., Wang, H., Keller, A.A., Wang, T., Li, F., 2014. The effect of humic acid on the aggregation of titanium dioxide nanoparticles under different pH and ionic strengths. *Sci. Total Environ.* 487, 375–380.